THE OPERATION OF THE FIRST SECTION OF THE NAL LINEAR ACCELERATOR

C. D. CURTIS, R. W. GOODWIN, E. R. GRAY, P. V. LIVDAHL, C. W. OWEN, M. F. SHEA AND D. E. YOUNG

National Accelerator Laboratory,† Batavia, Illinois, USA

The initial performance of the 10-MeV section of the NAL 200-MeV linear accelerator is presented. The pre-accelerator, mechanical and rf systems of the linac, beam transport lines, diagnostic equipment and computer-control system are described briefly. Beam emittance, profiles, momentum spread and operating linac parameters processed through the computer are displayed.

The maximum beam current accelerated to 10.4 MeV was 160 mA with a cavity transmission of 72 per cent. The phase-space density was significantly higher in the core of the beam than near the periphery. For a 150-mA beam the measured emittance areas including 80 per cent of the beam current were 10 and 15 milliradian-cm in the x and y planes respectively. The beam-emittance growth through the linac was measured and a graph showing variations occurring under different operating conditions is presented. The total momentum spread of the 10-MeV beam, independent of beam current, was 1.0 per cent for approximately 90 per cent of the beam. Further improvements in beam quality can be expected from optimization of linac parameters.

1. INTRODUCTION

A 200-MeV linear accelerator (linac) and 8-GeV booster synchrotron constitute the injection system for the 200 GeV synchrotron at the National Accelerator Laboratory (NAL). Construction of the first section of the linac was started in May, 1968 as a prototype to test the design and to allow the development of subsystems required in the final 200-MeV linac. Protons were first accelerated to 10 MeV on June 26, 1969. Improvements continued on the systems until December 11, 1969, when the equipment was dismantled for movement from the temporary to the permanent laboratory.

This linac is part of a collaborative effort with Brookhaven National Laboratory (BNL) and Los Alamos Scientific Laboratory (LASL) intended to increase the energy, beam intensity, beam quality and reliability of the Alvarez standing-wave linac and Cockcroft–Walton preaccelerator system. The NAL linac design is similar to that of the new 200-MeV injector for the alternating gradient synchrotron at BNL. The BNL drift tube and cavity specifications were adopted to save design effort and to allow early construction. These parameters are summarized in Table I.[1,2] The performance specifications of the NAL linac are given in Table II. There are notable differences between the detailed design features of the BNL and NAL linacs mainly arising from the different requirements

of the synchrotrons into which they inject. It is also planned to use the LASL scheme of resonant post-couplers to stabilize the rf fields more than in the conventional Alvarez structure.[3] This scheme will be used for the longer cavities beyond the first 10-MeV section and performance of the post-couplers will therefore not be reported in this paper.

2. DESCRIPTION OF 10-MeV SYSTEM

The ion source is a duoplasmatron with a plasma expansion cup. The design is still in a state of evolution, with three expansion cup geometries having been tested to date. Figure 1 is a drawing of the latest version, which has given our greatest accelerated beam current. The design is similar to one developed at the MURA laboratory except for modification of the expansion cup.[4]

The ion source injects directly into a 30-cm-long accelerating column which is designed with a convergent Pierce field to prevent expansion of a parallel beam due to space charge forces. This design is similar in principle to the BNL high-gradient column,[5] but with a lower maximum gradient of 33 kV/cm. There are seven accelerating gaps following an extraction gap. All electrodes are fabricated of titanium. The aperture in each electrode is 2.8 cm, which means that the maximum current of uniform density that can be accelerated to 750 keV as a parallel beam is 250 mA. The exterior of the vacuum envelope for the accelerating column is insulated by sulfur-hexafluoride gas at a

TABLE I

200-MeV linear accelerator specifications

Cavity Number		1	2	3	4	5	6	7	8	9
Proton energy in	(MeV)	0.75	10.42	37.54	66.2	92.6	116.5	139.0	160.5	181.0
Proton energy out	(MeV)	10.42	37.54	66.18	92.60	116.5	139.0	160.5	181.0	200.3
Cavity length	(m)	7.44	19.02	16.53	16.68	15.58	15.54	15.83	15.88	15.73
Cavity diameter	(cm)	94.0	90.0	88.0	88.0	84.0	84.0	84.0	84.0	84.0
Drift-tube diameter	(cm)	18.0	16.0	16.0	16.0	16.0	16.0	16.0	16.0	16.0
Bore-hole diameter	(cm)	2.0–2.5	3.0	3.0	3.0	4.0	4.0	4.0	4.0	4.0
Cell length L (First cell)	(cm)	6.04	12.2	41.1	53.3	61.8	68.2	73.3	77.6	81.3
(Last cell)	(cm)	21.8	40.8	53.0	61.5	67.9	73.1	77.4	88.1	84.3
Gap length G (First cell)	(cm)	1.30	4.4	12.2	19.5	22.6	27.1	30.9	34.3	37.3
(Last cell)	(cm)	6.70	12.7	19.3	25.1	26.9	30.8	34.2	37.1	39.7
G/L (First cell)		0.21	0.20	0.30	0.37	0.37	0.40	0.42	0.44	0.46
(Last cell)		0.31	0.31	0.36	0.41	0.40	0.42	0.44	0.46	0.47
Axial transit-time factor (First cell)		0.64	0.86	0.82	0.75	0.73	0.68	0.64	0.61	0.58
(Last cell)		0.81	0.81	0.75	0.69	0.69	0.65	0.61	0.58	0.55
Effective shunt impedance (First cell)	($M\Omega/m$)	27.0	53.5	44.6	35.0	29.6	24.8	21.5	18.9	16.7
(Last cell)	($M\Omega/m$)	47.97	44.8	35.2	28.5	25.0	21.7	19.0	16.8	14.9
Drift space following cavity	(m)	0.22	0.6	0.75	1.0	1.0	1.0	1.0	1.0	—
Number of full drift tubes		55	59	34	28	23	21	20	19	18
Average axial field	(MV/m)	1.60–2.31	2.0	2.60	2.60	2.56	2.56	2.56	2.56	2.56
Average gap field (First cell)	(MV/m)	7.62	10.0	8.7	7.03	6.9	6.4	6.1	5.8	5.6
(Last cell)	(MV/m)	7.45	6.45	7.2	6.3	6.4	6.1	5.8	5.6	5.4
Peak surface field (First cell)	(MV/m)	8.9	12.6	13.1	12.9	14.0	14.1	14.2	14.3	14.5
(Last cell)	(MV/m)	10.2	9.7	12.9	13.2	14.1	14.2	14.3	14.5	14.8
Cavity excitation power	(MW)	0.61	1.50	2.34	2.44	2.50	2.55	2.65	2.70	2.75
Total power per cavity for 100 mA	(MW)	1.58	4.20	5.20	5.08	4.90	4.79	4.81	4.75	4.68

Total accumulated length	144.8 m		Total cavity excitation power	20.0 MW
Total number of unit cells	286.0		Total linac rf power for 100 mA	40.0 MW
Total number of full drift tubes	277.0			

pressure of two atmospheres in a fiberglass and epoxy pressure vessel much like that of an earlier description.[6] A drawing of the column with the initial ion source in place is shown in Fig. 2. A photograph of the column in its operating position is shown in Fig. 3.

A 600-kV high-voltage power supply, modified for use to 800 kV, was loaned to NAL by Argonne National Laboratory. All the testing of the prototype preaccelerator and 10-MeV linac has been carried out using this high-voltage power supply.

The 750-keV beam-transport system is twelve feet in length, measured from the aperture in the last accelerating electrode of the column to the inner surface of the linac-cavity end wall. The layout shown in Fig. 4 is the system actually used in the prototype testing in contrast to the initial design.[7] Focusing is accomplished by three quadrupole triplet magnets each of which has the outer quadrupoles connected in series and the middle quadrupole independently adjustable.

TABLE II

200-MeV linear accelerator performance parameters

Output energy	200.30 MeV
Output momentum spread, total for 90% of beam	2.7×10^{-3}
Peak beam current	100 mA
Emittance at 200 MeV (each transverse mode)	1.5–3.0 mrad-cm
Beam pulse length	100 μsec
Pulse repetition rate	15 pps
Cavity resonant frequency	201.25 MHz
RF pulse length, variable to	400 μsec
RF duty factor, maximum	0.006
Synchronous phase angle, from rf peak	$-32°$

Operation has been with the focusing order in the horizontal plane *D–F–D*, *F–D–F*, *D–F–D* preceding a *D* quadrupole in the first half drift tube of the linac.

The transport system was designed with the aid of the BNL computer transport program of R.
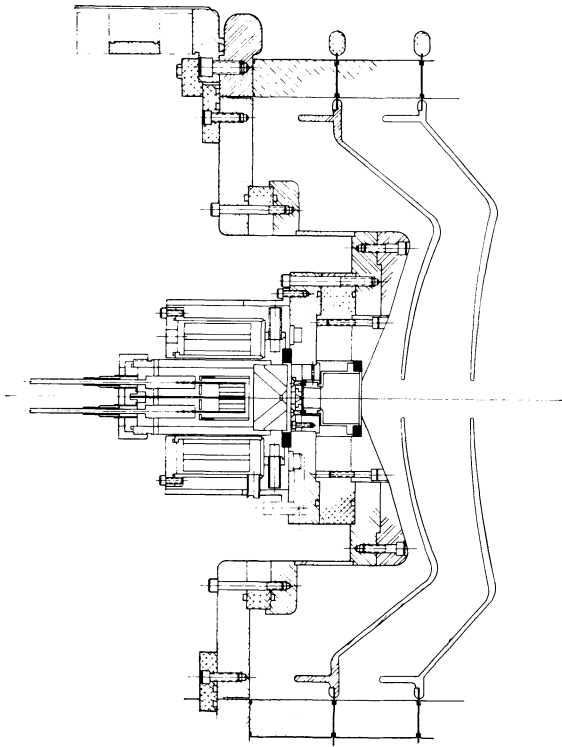
FIG. 1. Ion source.

Chasman.[8] The lengths of the quads are 12–24–12 cm for each of the first two triplets and 8–16–8 cm for the third triplet. The iron-to-iron spacing of all quads is 2 cm and the aperture is 8 cm in diameter. The fields are dc and have been operated most often at strengths between 300 and 400 G/cm in the first two triplets and 500 to 700 G/cm in the third triplet. Beam diagnostic equipment located in the transport line includes four beam current toroids, horizontal and vertical emittance probes at each of two locations and adjustable collimating slits at the entrance to the linac.

The buncher was a single-cell resonant cavity constructed from the copper-plated steel buncher cavity used originally with the University of Minnesota linac. The internal elements were replaced by a slug tuner, a drive loop, and two half drift tubes (all OFHC copper). The electrical characteristics of the cavity were calculated using the MESSYMESH linac field computational program.[9] Excitation power was from a 15dB directional coupler in the drive line which supplied rf power to the 10-MeV cavity. Phase and amplitude were adjusted with mechanical phase shifters and a hybrid junction attenuator.

The 10-MeV accelerating cavity (Figs. 5 and 6) is made of copper-clad steel and is pumped by three 1200-liter/sec ion pumps.[10] The cavity normally operates at a pressure of 2×10^{-7} torr. Each cavity is temperature controlled by water flowing in cooling channels welded to the steel structure.

The drift tubes are fabricated according to dimensions calculated by the MESSYMESH program[9] and are dimensionally identical to the BNL drift tubes. Drift tube quadrupoles are pulsed. The cavity begins and ends with a half drift tube. The loaded Q is 60,000, 89 per cent of the theoretical value calculated with no corrections for openings such as pumpout ports and pickup loops.

The 10-MeV cavity was designed to have a large tilt in the electric-field gradient. This tilt is achieved by tuning the low-energy end at a calculated frequency above the operating frequency and the high-energy end below the operating frequency by the same amount. RF fields in the cavity were measured using perturbation techniques[11] with an on-line computer. Figure 7 is a plot of the normalized gap fields along the tank as they were finally adjusted. The rf system is a driven amplifier, rated at 5 MW output power, and is described in detail in the block diagram shown in Fig. 8. The power-amplifier tube is an RCA 7835 triode used in an amplifier circuit.[12] The anode voltage for the final amplifier is supplied from a hard-tube modulator that also serves as the active element for the cavity voltage-control servo system.

The transport system for the 10-MeV beam is shown in Fig. 9. This system contains beam-current toroids, horizontal and vertical emittance probes, a quadrupole doublet, the object slit for a 60° analyzing magnet and segmented beam-width monitors both upstream and downstream from the analyzing magnet. The downstream monitor is located at a position focus and provides a means of measuring the momentum spread of the linac beam.

The control system for the 10-MeV accelerator is developed around a 16-bit control computer,[13] a television display scope with alphanumeric and graphic capability, a storage scope and a complete complement of computer peripherals. Primary emphasis for this system has been directed toward data acquisition and control of equipment useful in beam-diagnostic and accelerator-research experiments. The computer assembles information
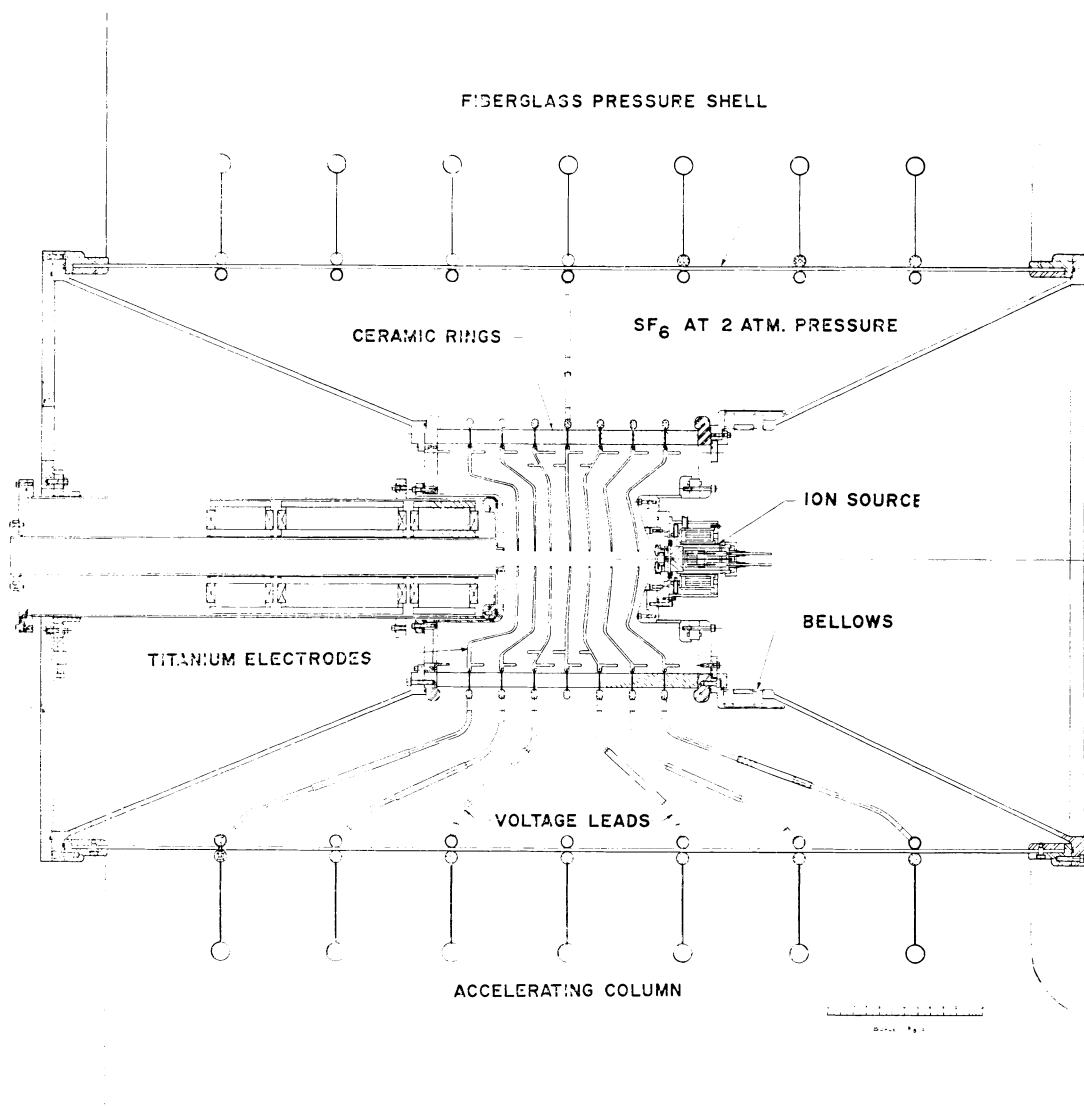
FIG. 2. Accelerator column and ion source.

from the various components as commanded by programs called into memory from the magnetic disc and prepares displays of the assembled information for the operator. Set-point control of an accelerator parameter can be accomplished by typing the desired value onto the display scope from a keyboard. Continuous variation of any controlled parameter is possible through a single shaft-encoder knob whose function and sensitivity are preselected by the operator. As this knob is adjusted, the value of the selected parameter forms the abscissa of a graph plotted on the storage scope. The ordinate of this graph can be the value of any parameter measured by the computer. In this way, for example, 10-MeV beam current may be plotted as a function of preaccelerator transport quadrupole field.

During the period of operation of the 10-MeV section, all drift-tube quadrupoles and beam-line steering, focusing and bending magnets were controlled and monitored through the computer. In order to document the operating parameters rapidly, a program was written that allowed the operator to request a 'linac log' to be printed on a high-speed printer. An example of this output is shown in Table III. The computer gathers data

for twenty machine cycles and gives as output the average value and the standard deviation (in parentheses) of each parameter shown in the table. The log is produced in about 5 seconds.

The emittance of the beam in the 750-keV and the 10-MeV beam transport system was measured with the computer-controlled probe and data acquisition system shown in Fig. 10. The 750-keV probe consists of a narrow (0.075 mm) slit, a 10-cm drift space and a segmented current-pickup plate that has 20 segments on 0.2 mm centers. An individual segment thus corresponds to two milliradians angular divergence. The dimensions of the 10-MeV probe are scaled appropriately to maintain the same angular resolution. Under program control, the computer positions the slit and steps it across the beam. Analog signals proportional to the amount of current incident on each segment are amplified, sampled and held at a preselected time at each slit position. These signals are then digitized and fed into the computer. Immediately following the beam scan, the computer calculates for a preselected intensity threshold the phase-space area and fraction of the total beam contained within this area.

Input parameters for the program and the results of the calculations are transmitted between the operator and the computer via the alphanumeric display scope. Graphic representation of the results of the measurement are presented on the storage scope. A photograph of this display is
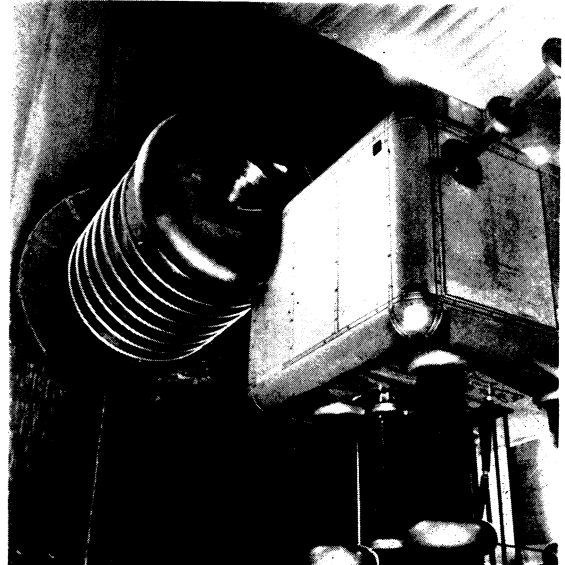
FIG. 3. Photograph of column in operating position.
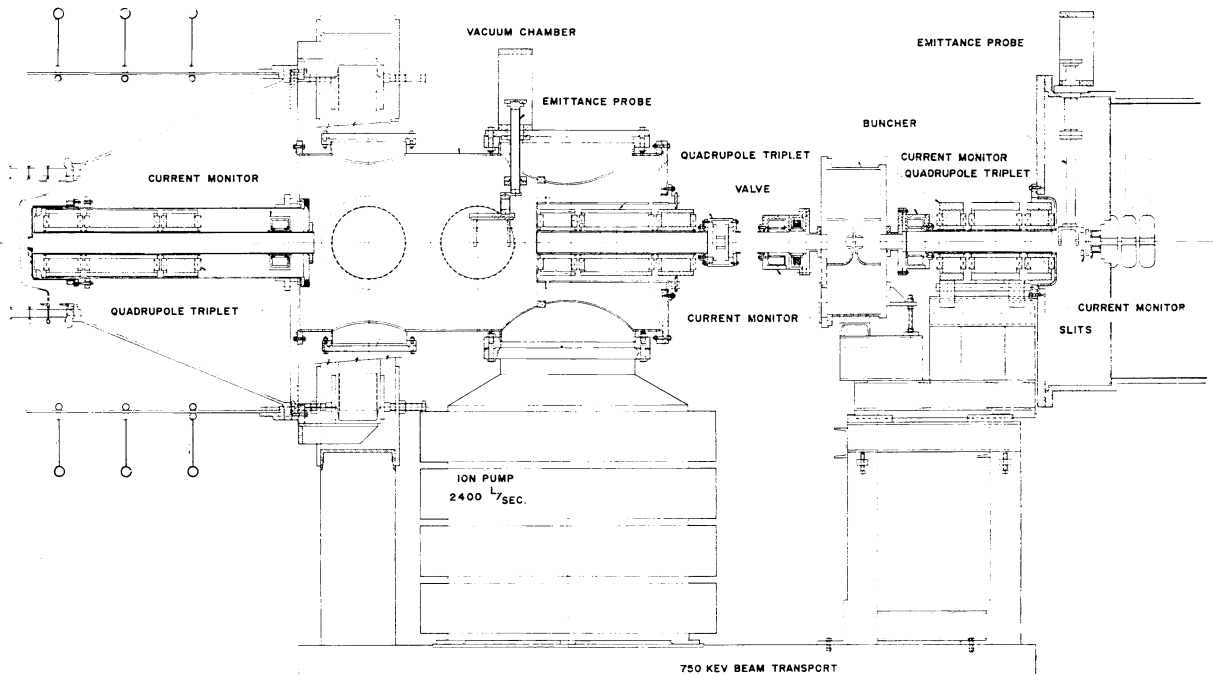

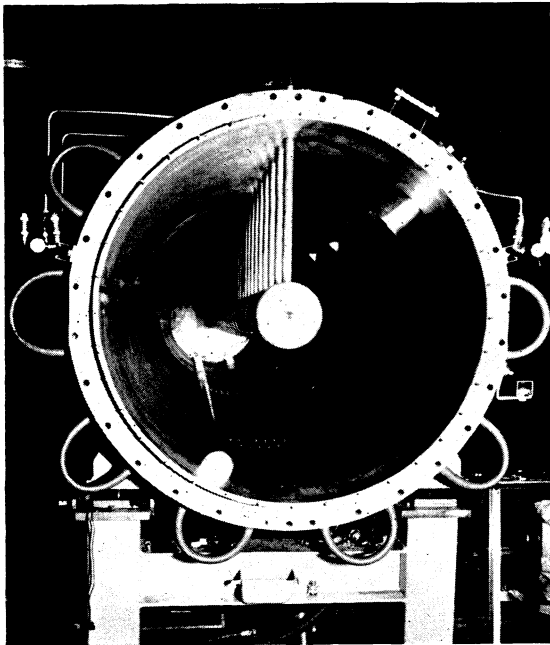FIG. 4. 750-keV beam transport line.
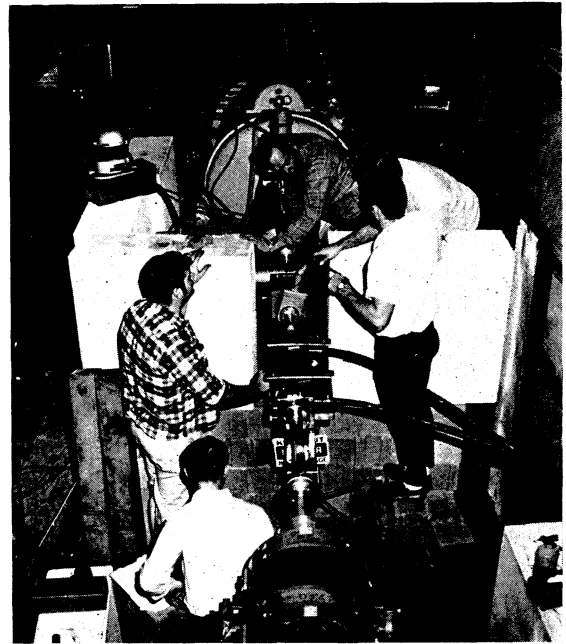
FIG. 5. Inside view of linac cavity.

FIG. 6. View of 10-MeV area of linac.

shown in Fig. 11. The isometric representation is
a plot of slit position (shown horizontally) versus
angle, with the third coordinate of the points
proportional to current measured on the individual
probe segments. The intersection of the plane with
the three-dimensional surface is the usual two-
dimensional phase plot, shown in the upper-left
corner of the photograph. The computer repeti-
tively calculates the phase-space area and the
percentage of beam contained within this area, and
plots the results along with the associated axes in
the upper right. Also shown are the spatial dis-
tribution (beam profile) and angular distribution.
The beam current averaged over the run, the full
width at half maximum, center of gravity (in cm)
and the area and per cent of beam associated with
the two-dimensional phase-space plot are listed
in the lower left. The threshold (as a fraction of
the maximum individual segment current detected),
which determines the vertical location of the plane
on the isometric, is preselected by the operator.
A change of this input parameter allows the operator
to see the shape of the two-dimensional phase-space
plot for various beam percentages. The program
allows for the sequential operation of up to four
preselected probes without operator intervention.
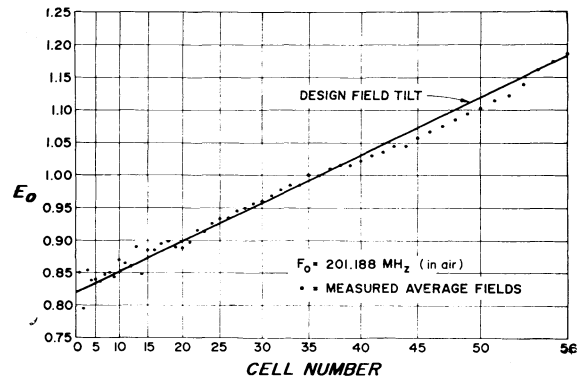Incoming emittance data from each probe are

FIG. 7. Comparison of measured and design fields
in 10-MeV cavity.

automatically stored on the magnetic disc to allow
subsequent recalculation and display of the data at
various thresholds. These data then can be stored
on magnetic tape for later retrieval and analysis.

With this system, the beam is interrupted for only
a few seconds while the data are being acquired.
An additional 20 seconds are required to perform
the calculations and to present the graphic display
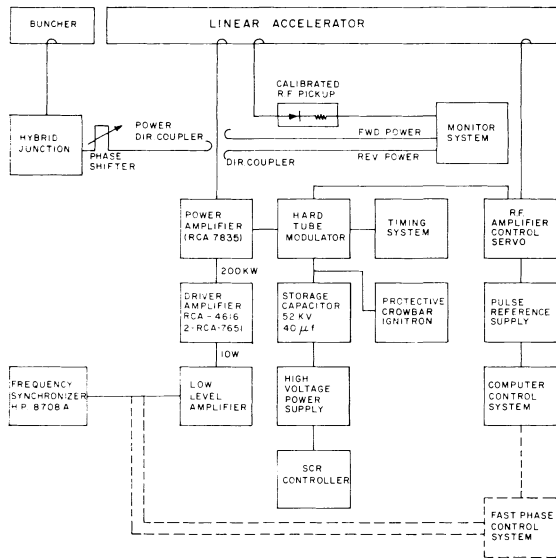on the storage scope.

FIG. 8. Block diagram of rf system.

3. PERFORMANCE

A. *Preaccelerator and Beam Transport*

During a brief period of operation on a test bench, the ion source of Fig. 2 gave beam currents up to 300 mA. Measurement of the source emittance by use of a slit plate and a fluorescent screen gave an approximate value of 22 mrad-cm for a current of 250 mA at 70 keV.

With this source mounted on the accelerating column and with the design value of 40 kV across the extractor gap, one would expect to accelerate to 750 keV a parallel beam of 32 mA, the plasma cup being 1.0 cm in diameter. The beam actually accelerated was approximately 35 mA. To accelerate 250 mA under the same conditions requires a much larger area of plasma surface. To achieve this without the development of a larger plasma-expansion cup, the column was operated with the first gap, the normal extraction gap, shorted. Extraction then took place in the second gap while the first gap was used as a further plasma-expansion region. Beam currents up to 260 mA were accelerated through the column in this manner. This mode of operation represents, of course, a departure from the original Pierce geometry.

In an attempt to provide a large plasma surface area in a Pierce geometry, the plasma-expansion cup of the source was scaled linearly in all dimensions to a diameter of 2.8 cm. This modification gave some improvement in performance, but not

as much as a second modification to the cup that allowed a longer drift distance for plasma expansion. This latter change, shown in Fig. 1, provided the beams on which most of the performance data in this report are based. Development of the ion-source cup geometry is continuing, because this

TABLE III

Printout of 10 MeV linac parameters as monitored by the computer control system

```
LINAC LOG 12/11/69  0028
TANK1 TRANSMISSION           68.6 %
  TANK1 RF LEVEL AT BEAM TIME .998 (.003)
  TANK1 RF LEVEL......       1.063(.001)
  BEAM TOROIDS: SOURCE OUT   296.6(5.72) MA
               BUNCHER IN    267  (7.43) MA
               BUNCHER OUT   261.5(7.93) MA
               LINAC IN      218.5(5.87) MA
               LINAC OUT     150.1(6.23) MA
               10 MEV #2     3.277(.401) MA
               10 MEV #3     1.257(.852) MA
  HIGH VOLTAGE............   746.5(.586) KV
  750 KEV QUADS: QTM1 ENDS  329.7(.063) G/CM  326.3
                 CENTER     358.3(.067) G/CM  353.5
            QTM2 ENDS       391.1(.419) G/CM  389.1
                 CENTER     313  (.036) G/CM  308
            QTM3 ENDS1      260.3(.036) G/CM  519.7
                 ENDS2      263.7(.043) G/CM
                 CENTER1    298.9(.068) G/CM  598.6
                 CENTER2    289.4(.068) G/CM
  10 MEV QUADS: DOUBLET #1  409.1(4.96) G/CM  392.1
               DOUBLET #2   469.5(5.75) G/CM  460.6
  STEERING MAGNETS: X.....   .545 (.071) MR    -.006
                    Y.....   .351 (.046) MR    .004
  SPECTROMETER MAGNET        .962 (.001) AMPS  .95
  PRESSURE: 750 TRANSPORT   2.691(.025) UTORR
            TANK1           .875 (.015) UTORR
  PROBES: EMITTANCE #1       .631 (.001) CM
                    #2       .515 (.001) CM
                    #3       .957 (.001) CM
                    #4       .559 (.001) CM
                    #5       .387 (.002) CM
                    #6       .462 (.001) CM
        10MEV SLIT         6.759(.001) CM
        WIDTH MONITOR       .522 (.001) CM
        10MEV CUP          9.722(.004) CM
  TANK1 QUADS: P.S.#1       97.87(.012) AMPS  98.29
                    #2      220.6(.02 ) AMPS  216.3
                    #3      212.4(.014) AMPS  212.4
                    #4      208.4(.016) AMPS  208.4
                    #5      197.8(.037) AMPS  204.5
                    #6      175.8(.026) AMPS  178.5
                    #7      177.6(.019) AMPS  176.1
                    #8      174.1(.01 ) AMPS  173.8
                    #9      168.9(.015) AMPS  169.9
                   #10      164.9(.013) AMPS  167.1
                   #11      160.1(.745) AMPS  164.1
                   #12      228.3(.567) AMPS  230.9
                   #13      226  (.041) AMPS  228.1
                   #14      222  (.851) AMPS  224.8
                   #15      221.1(.07 ) AMPS  221.2
                   #16      215.6(.044) AMPS  218
                   #17      214.7(.011) AMPS  214.8
                   #18      210.1(.053) AMPS  210.7
                   #19      207.5(.041) AMPS  208.1
                   #20      204.8(.006) AMPS  204.9
                   #21      148.4(.069) AMPS  150.5
                   #22      148.9(.011) AMPS  149.7
                   #23      148.7(.063) AMPS  148.8
                   #24      145.4(.01 ) AMPS  147.5
                   #25      145.6(.014) AMPS  146.3
                   #26      139.3(.073) AMPS  144.5
                   #27      141.7(.01 ) AMPS  143.7
                   #28      142.7(.014) AMPS  142.8
                   #29      140  (.013) AMPS  141.6
                   #30      139  (.011) AMPS  140.7
                   #31      137.8(.016) AMPS  139.4
                   #32      138.6(.02 ) AMPS  138.6
                   #33      119.7(.01 ) AMPS  120.5
```
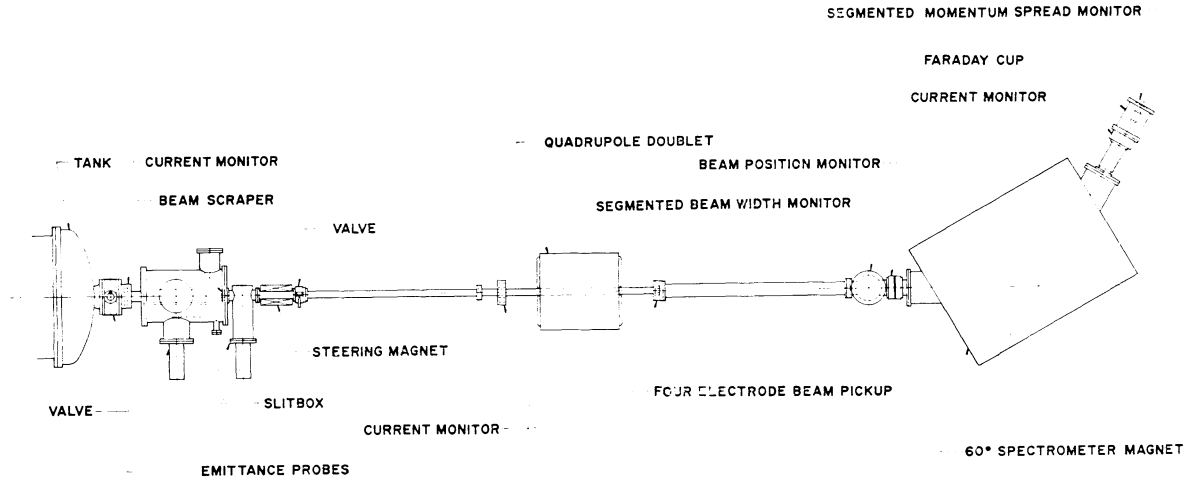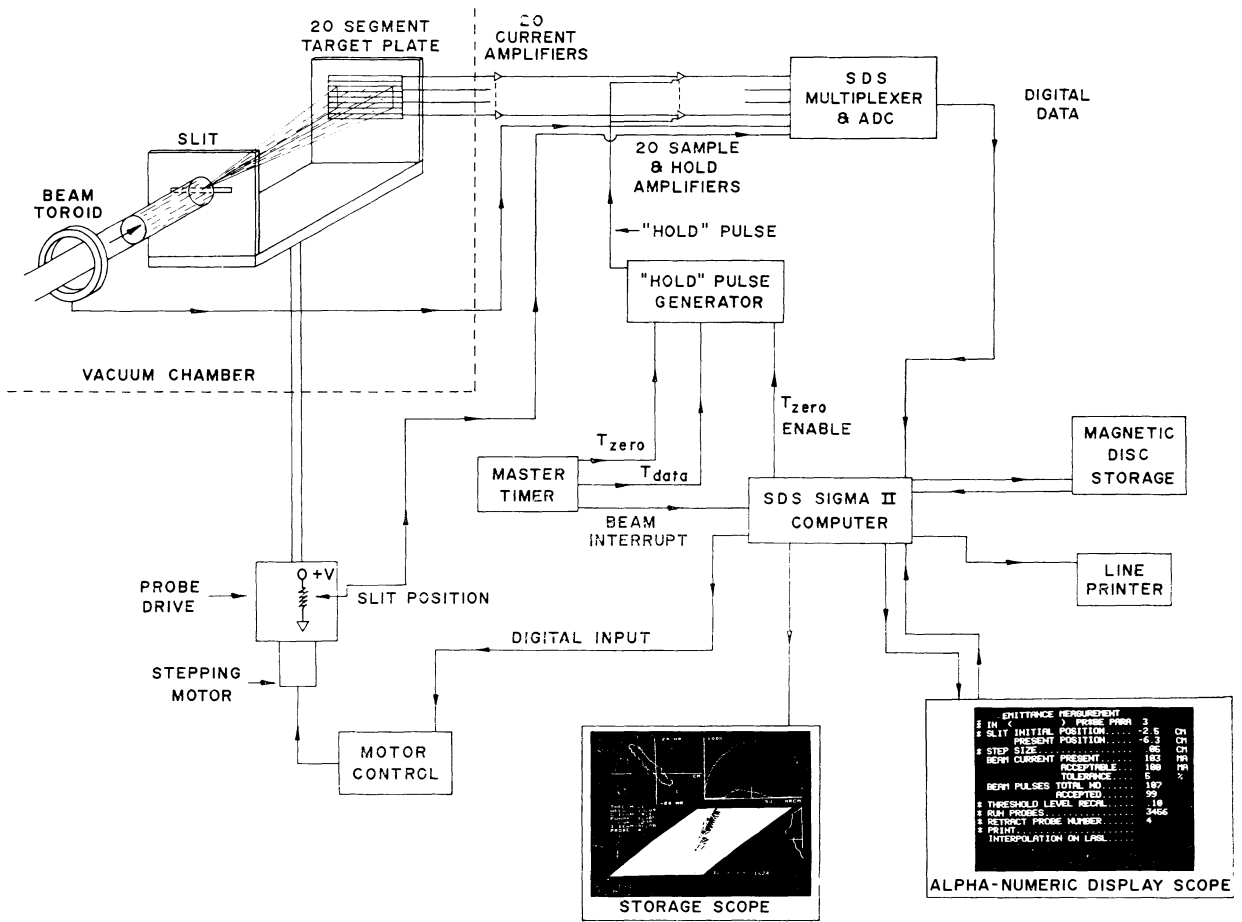
C. D. CURTIS *et al.*

FIG. 9. 10-MeV transport system.

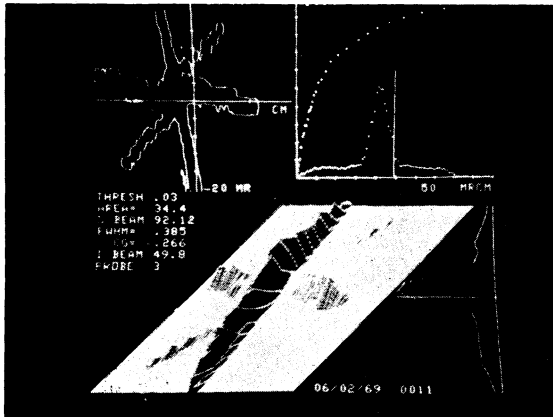FIG. 10. Emittance measuring equipment.

FIG. 11. Emittance and beam profile plots for *x* motion at linac input, showing three ion components in the beam. Protons constitute the most sharply focused component.

latest configuration has provided only about 150 mA in the nominal Pierce field distribution. As before, shorting of the normal extraction gap permitted higher beam currents, up to 320 mA, to be accelerated. The column was always operated in this manner, even for low beam currents, in the collection of the data given in this report.

The mass ratio of ions in the beam from the column is a strong function of the arc current in the source and a lesser function of the magnetic-field intensity. The proton percentage typically varies from 50 per cent to over 90 per cent as the arc current varies from 15 A to 35 A. After the beam has passed through one or more magnetic triplets, the different mass components have different orientations in phase space. One can therefore estimate approximately the proton percentage by examining the beam profile distributions in comparison with the isometric plot of intensity in transverse phase space. Figure 11 shows the survival of three mass components near the input of the linac at a relatively low total beam current. In most cases, low arc currents in the source were used to obtain low beam currents, which consequently had low proton percentage.

Emittance measurement was affected by presence of the multiple-ion beams. The true proton beam emittance is smaller than the plotted value at each point of the percentage of beam versus emittance curve, especially at the higher beam percentage points. This effect becomes less pronounced at high beam currents because of smaller molecular-ion content.

Emittance measurements for a focused beam were taken at various times during a long beam pulse. The current decreased from 116 mA at a time early in the pulse to 70 mA at a time 60 μsec later. These measurements showed that the emittance ellipse rotated very slightly during the pulse. In addition, the relative proton content dropped 65 to 50 per cent because of the simultaneous decline in the arc current. At larger beam currents (250 mA), the ellipse rotated noticeably during the pulse. This rotation could be accounted for by a drop in the preaccelerator voltage that occurred because there was no voltage-stabilizing bouncer.

Emittance and beam-profile measurements are made at the input and output of the linac during performance tests at a variety of beam currents and operating conditions. Figure 12 shows an example of these measurements in the horizontal and vertical planes at a distance 17 cm upstream of the linac entrance. The effect of the buncher, particularly on the vertical emittance, can be seen because there are two sets of measurements under similar operating conditions, one with buncher on and one with buncher off. The total beam current out of the column, including molecular ions, was 170 mA. A similar effect was present for both higher and lower beam currents and appears to be the result of a change in focusing of the beam in the third triplet with change in energy by the buncher.

The emittance and beam density distribution reproduce extremely well from one time to another under identical operating conditions. There is a significant variation for different operating conditions, however. In Fig. 13 are plotted the emittance curves for horizontal and vertical motion at the input to the linac when the data from nine runs under different operating conditions are averaged. High-current runs ranging from 250 mA to 290 mA were selected to minimize the effect of molecular-ion content. The spread in emittance represents the extreme variation between runs. A run with lower emittance at one beam-percentage point tends to have lower emittance at the other percentage points as well. A plot of raw emittance data versus beam current from 27 runs shows the emittance to decrease slowly with decreasing beam current. Trimming of several emittance plots at 100 mA to eliminate most of the molecular ions resulted in a reduction of the emittance values to approximately 50 per cent of those at 270 mA. The average data for these plots after trimming are also shown in Fig. 13.

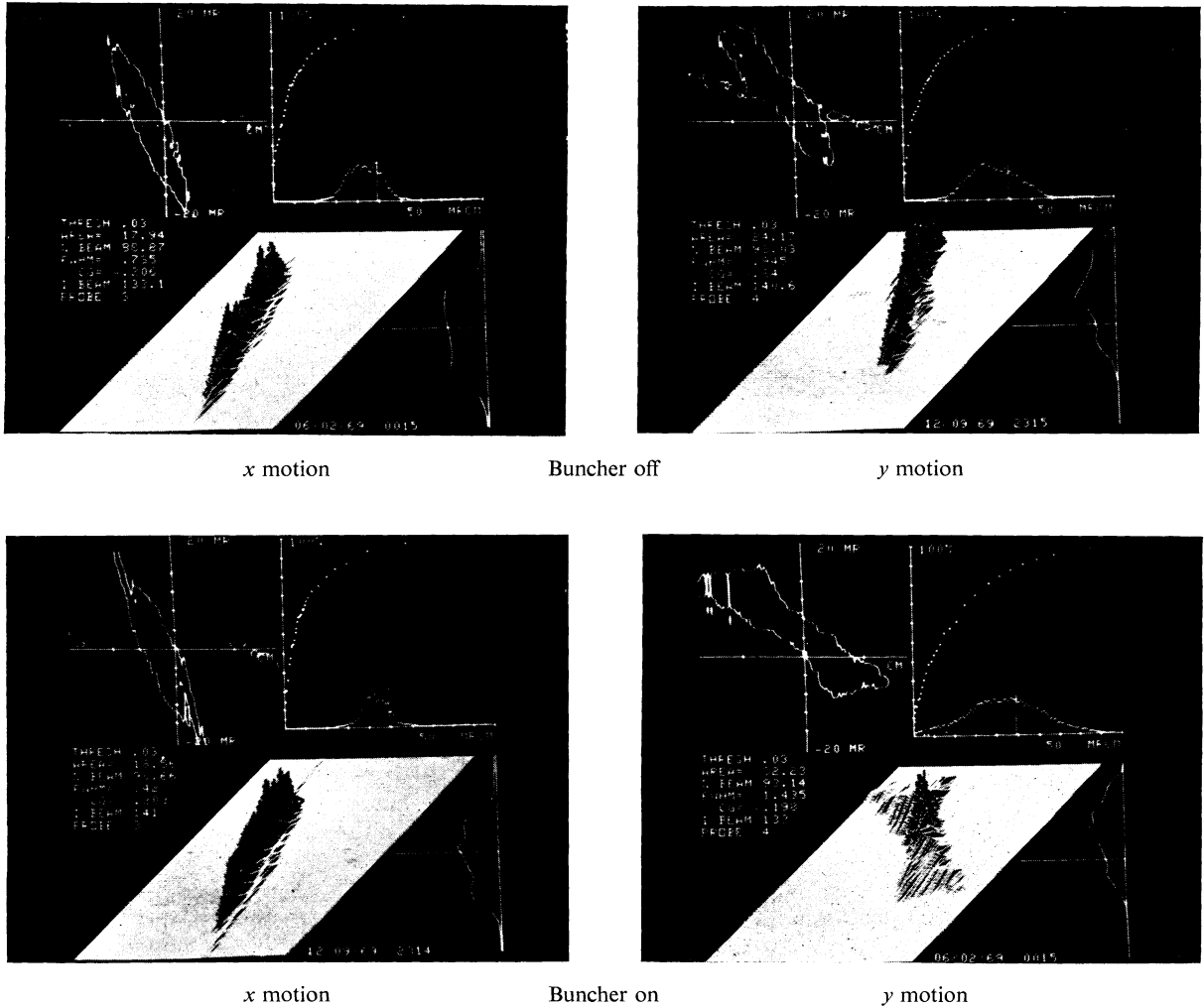A remark is in order with respect to the inter-

x motion   Buncher off   y motion

x motion   Buncher on   y motion

FIG. 12. 750-keV beam through buncher.

pretation of emittance and beam profile plots. The angular distribution in $x - x'$ space represents a sum over $y - y'$ space (and vice versa), because the slit for horizontal measurements extends vertically across the entire beam. In addition, for a beam of circular cross section of radius r and uniform density, the distribution of particles as a function of displacement x from the center becomes a convex plot with intensity proportional to $\sqrt{[1 - (x/r)^2]}$.

An example of beam-current readings from toroids at various points in the 750-keV transport line is given in the top part of Table III. Loss of beam between the buncher and linac comes from some rake-off at the entrance to the linac. At high-beam current, adjustment of the triplets for greater

linac input beam than that shown in the table did not give maximum 10-MeV beam.

Emittance plots in both planes for a high-current beam at the input of the linac with the buncher off are shown in Fig. 14a and 14b. Some distortion in the phase plane is apparent. At lower beam currents, the ends of the emittance ellipse occasionally develop hooks which have relatively low-beam intensity in them, in contrast to the situation at high currents where distortions may affect a greater fraction of the beam.

B. *Linac*

During testing of the linac over a wide range of beam currents, many of the operating parameters

FIG. 13. Percentage of beam versus emittance area.

Other linac data logs show the following maximum accelerated beam achieved: 294 mA from column, 222 mA into linac, 160 mA at 10 MeV for 72 per cent transmission. Whether higher source current could give still more accelerated beam was not established.
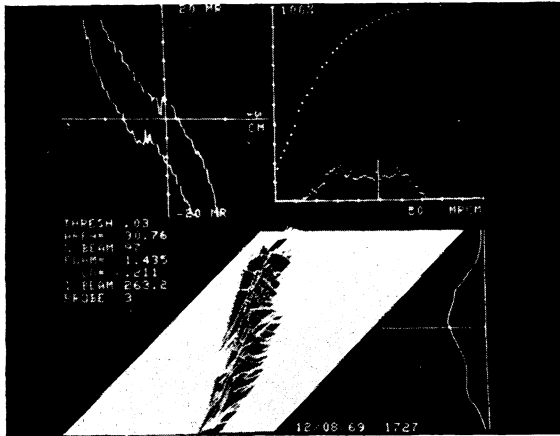
The maximum beam accelerated with the buncher off has been 75 mA. An example of 10-MeV beam emittance for a current of about 60 mA with buncher off is given in Fig. 14(c) and 14(d), where the tank transmission was 25 per cent.

Figure 15 shows emittance and profile plots for a 10-MeV beam at 150 mA. Similar data were collected at various beam currents. A plot of some of the data in Fig. 16 shows variation of emittance with beam current, as well as some scatter from run to run under somewhat different operating conditions. One will note the larger emittance area in the vertical plane compared to the horizontal plane for a comparable percentage of the beam. In addition, the variation of emittance with beam current is less strong in the vertical plane ($\sim I^{1/4}$) than in the horizontal plane ($\sim I^{1/2}$). These differences must result, in part, from the large effect on the vertical motion by the buncher, shown in Fig. 12. The areas in the two planes can be compared in another way by plotting the percentage of beam versus the emittance area, as shown in Fig. 13 at 150 mA.
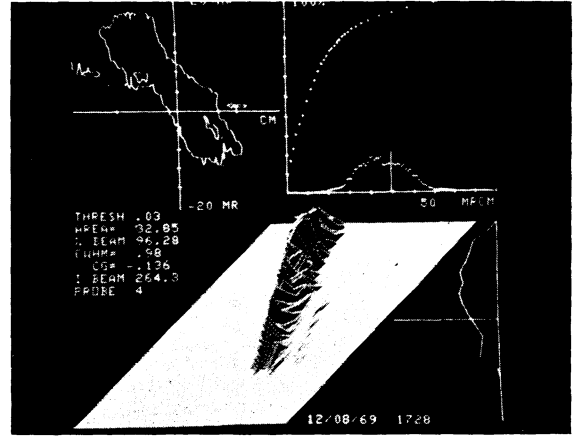
Of great interest and concern is the possible increase in normalized emittance (or loss of brightness) of the beam in passing through the first section of the linac.[14] Although a systematic investigation of the factors affecting emittance growth has not been made, it is of interest to determine what growth can be found in the existing data.

For each calculation of the emittance display, the values found for the curve of beam percentage versus emittance are stored for each emittance-measurement probe. From these data, a simple interpolation allows a comparison to be made between emittance areas containing the same fraction of the beam. An indication of beam growth between measurement-probe positions is then given as a graph (see Fig. 17) of the ratio of these emittance areas versus the beam percentage in both the horizontal and vertical planes.

The beam growth value is dependent on the beam density distribution. Furthermore, extraneous particles, such as other mass species in the 750-keV line, will introduce error in the growth ratio. This effect is particularly noticeable at the high beam percentages, where a significant increase in emit-
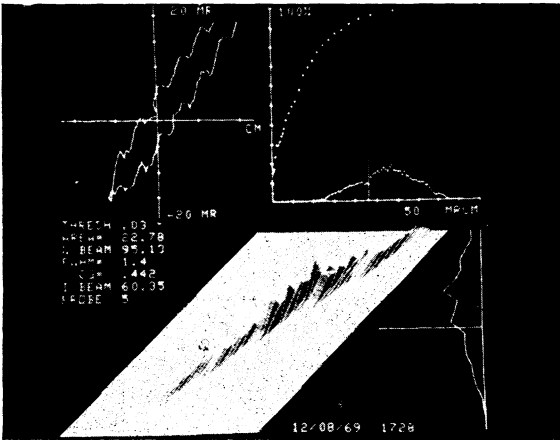
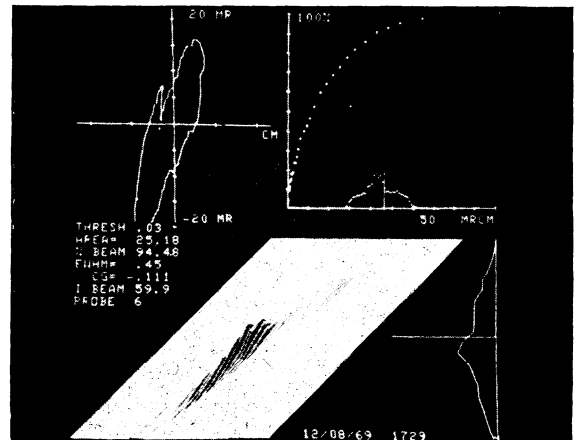of the system were continually monitored by the computer and various data logs were printed out on command. An example of one such log is Table III. One sees in this instance that the tank rf power level is near the nominal or design level (1.00) and the preaccelerator voltage is 746 kV. With a total ion beam of 296 mA from the column and 218 mA ($\geqslant$ 95 per cent protons) into the linac, the linac accelerated 150 mA to full energy of 10.4 MeV, for a transmission of 68.6 per cent. The tank quadrupoles are set at their 'nominal' value calculated assuming that injection of the beam into a second linac cavity would take place immediately. Consequently, beam toroids No. 2 and No. 3, some distance downstream measure much smaller current.

For some experiments, low-current beams in the range of 5–40 mA were rendered parallel so that all the current could be transmitted through the spectrometer magnet into a cup approximately ten meters distant (Fig. 9). Adjustment of the last six quadrupoles in the tank away from their nominal settings to accomplish a parallel beam resulted in a reduction in beam transmission by about one-third.

x motion   Beam through buncher (buncher off)   y motion
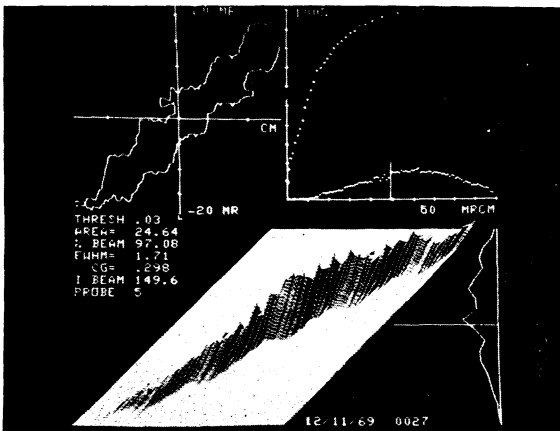

x motion   10.4 MeV beam   y motion
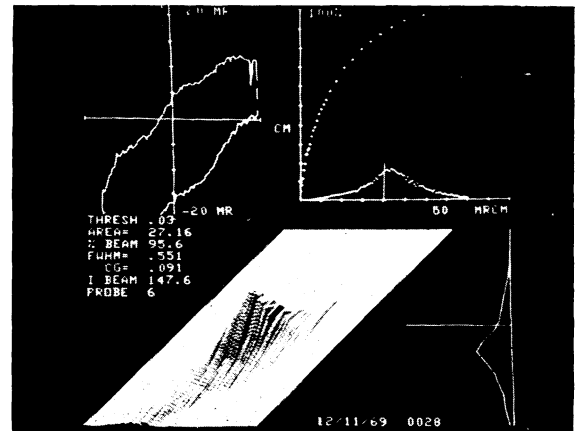
FIG. 14. Emittance displays at entrance and exit of linac.

x motion   y motion

FIG. 15. Emittance and profile plots for 150 mA at 10.4 MeV.

tance area can be seen. To decrease the effect of the extraneous particles, a trim correction was made that effectively limited the emittance calculation to a selected region of the emittance diagram. This simple correction makes it possible to delete the data resulting from extraneous particles that are clearly separated from the main beam.
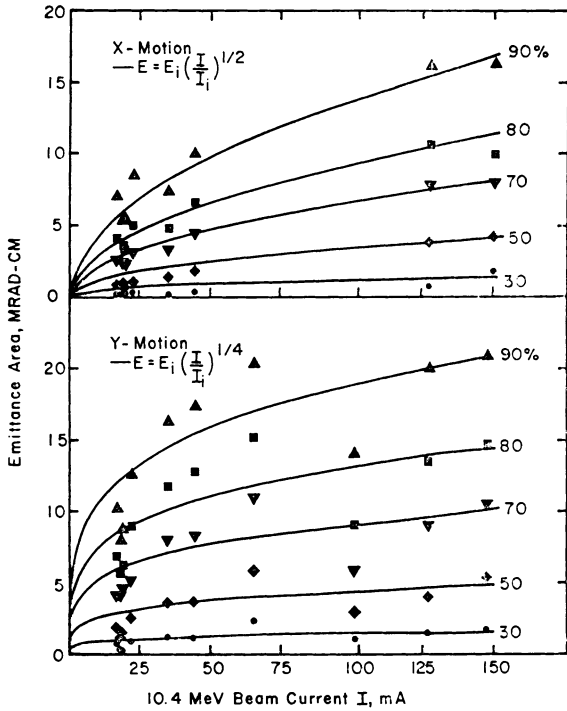
FIG. 16. Emittance versus beam current at 10 MeV

An example of growth as it appears on the storage scope is shown in Fig. 17 for passage of the beam through the linac, and also for passage through the 750-keV transport line. A summary of such trimmed beam growth values is shown in Fig. 18 for various accelerated beam currents. Values are plotted for both the x and y planes, using emittances corresponding to 40, 60, and 80 per cent of the beam current. At high beam currents, only y growths could be measured because of a malfunction of the x probe. At the side of the graph are shown several special growth ratios. These values resulted from comparing 10-MeV beam data taken with the buncher on to 750-keV data taken with the buncher off. These runs were taken consecutively to insure operating conditions as nearly identical as possible. The increased size of the growth shows the growth due to the buncher as well as the linac tank.

It should be noted that the beam was not matched into the cavity in the most desirable way, because a quick procedure was used to tune for maximum accelerated beam. The result is that the emittance areas are not equal in the x and y planes, nor do the beams have the correct size ratio to maintain the maximum size of the beam in the linac equal in both planes.

A segmented current pick-up plate at the end of the 10-MeV transport line (Fig. 9) monitors the momentum spread of the beam. Figure 19 shows storage-scope displays of the momentum distribution at three beam currents. Little current falls outside a one-percent spread, and there is little change with increase in beam current. There is also little difference in spread with buncher on and
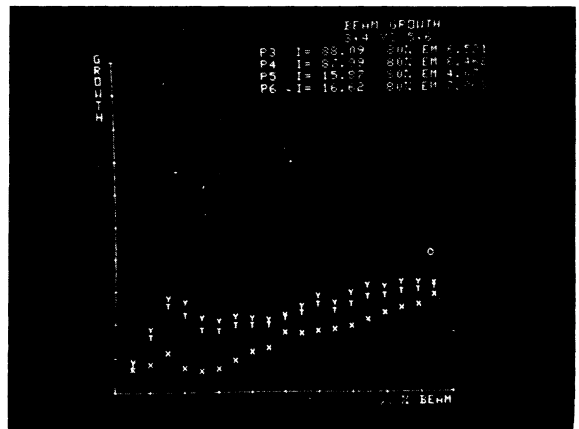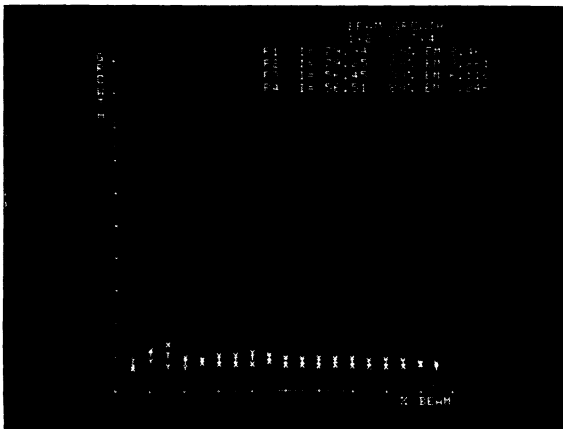
Sample 750-KeV transport growth

Sample 10-MeV accelerator growth

FIG. 17. Emittance growth displays through 750-keV transport and through 10-MeV accelerator.
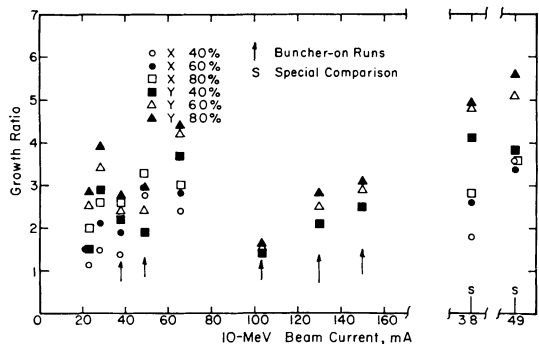
FIG. 18.   Beam growth through linac.

32 mA

100 mA

150 mA

FIG. 19.   Momentum spread at 10 MeV at various beam currents.

buncher off.   Close inspection of the momentum distribution shows that there is a continuum of beam with secondary peaks of very low intensity extending to low energy.

The longitudinal acceptance of the linac was briefly investigated by varying the energy of the preaccelerator at various cavity rf levels and measuring the transmission through the cavity (i.e., the ratio of the beam current out of the accelerator, as measured by the output toroid, to the current into the first half drift tube, as measured by the input toroid).   A comparison of these data with those predicted from beam-dynamics studies using the PARMILA program[15] showed that the shape of the variation of acceptance vs. preaccelerator voltage curves at various rf levels fits the predicted shape reasonably well (Fig. 20).   The reason for the discrepancy between the measured and computed values (approximately 5 per cent) has not as yet been determined, but could be attributed to an error in the cavity rf-loop calibration.

C. *rf System*

The initial operation of the rf system and the rf conditioning of the linac cavity have been reported elsewhere.[7]   Figure 21 shows the waveforms of the linac cavity voltage and reflected power in the transmission line under conditions where the amplitude servo loop is open or closed.

With 150 mA accelerated in the 10-MeV cavity, the cavity voltage was depressed by 15 per cent during the beam pulse.   This loading is compensated by exciting the cavity to a higher level before the beam comes on.   No attempts have been made to improve this situation by varying the coupling or the match to the loaded cavity or to adjust the feedback characteristics of the cavity-voltage servo.
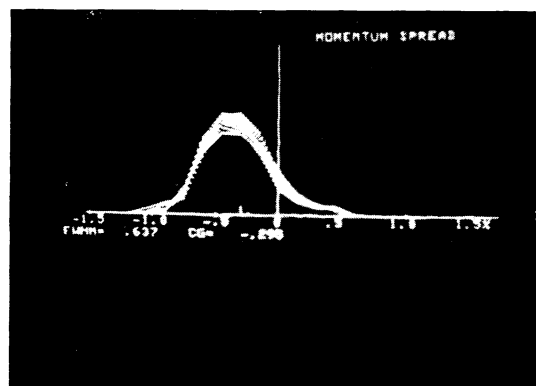
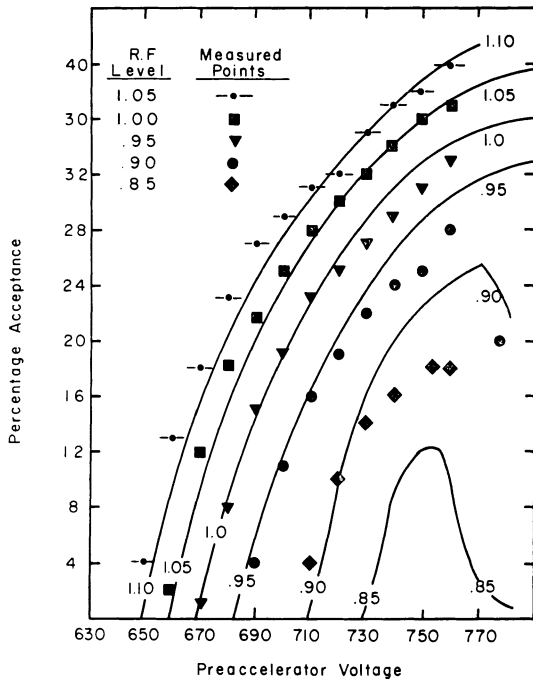Figure 21 also shows oscilloscope pictures of
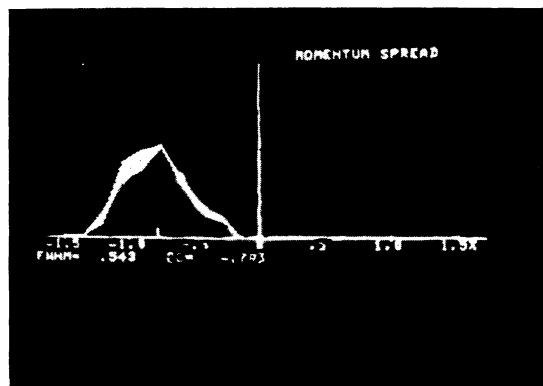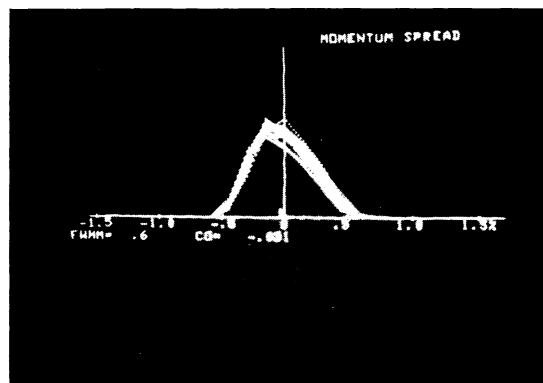
FIG. 20. Linac acceptance as a function of pre-accelerator voltage.

the forward and reverse power from the power amplifier to the cavity with 150 mA beam accelerated. It is apparent from these pictures that the match to the unloaded cavity is good and that the power amplifier is producing additional power during the beam pulse that is of the correct magnitude to compensate for the beam loading. The match during the beam pulse could be improved by adjusting the length of transmission line and cavity coupling. This would necessarily, however, be at the expense of a poor match to the unloaded cavity.

4. SUMMARY OF PERFORMANCE

The beam characteristics of the 10-MeV section of the NAL linac have been measured. Maximum beam current accelerated to 10.4 MeV was 160 mA with an input beam of 222 mA giving a tank transmission of 72 per cent. Measurement of the rf power delivered to the beam confirmed the current measurement.

For a 150 mA accelerated beam the measured emittance area was 16.5 mrad-cm in the x plane and 21 mrad-cm in the y plane for 90 per cent of the beam. The phase-space density increased sharply toward the core of the beam at both the entrance

and the exit of the linac. Emittance of the 10-MeV beam varied approximately as the square root of the current in the x plane and less strongly in the y plane. This difference may result from the observed smearing out of the y-plane emittance (a 'blownup' projection of the six-dimensional hypervolume) during passage of the beam through the buncher and the following triplet.

Growth of the emittance area of the beam was observed for a range of intensities. The amount of growth was dependent upon the operating conditions and varied from a value of 1.5 to 4.5. There was a trend toward less growth for the lower-percentage contours corresponding to the core of the beam. There was no real evidence for increased growth with increasing beam current. An additional growth was observed between the buncher and linac, particularly in the y motion, by as much as a factor of two. It is apparent that adjustments are required in the transport line and buncher to improve this situation.

Total momentum spread under normal operating conditions was approximately 1.0 per cent, independent of beam current.

Comparison of measured and computed phase acceptances have shown fair agreement. Calculations of ouput-beam properties are being made using the PARMILA beam-dynamics program that includes the effects of space-charge forces for measured input-beam characteristics. For a typical linac operating condition, preliminary results show an emittance growth observable in the regions outside the central core.

Improvements in the quality of the 10-MeV beam can be expected when optimum operating conditions are achieved.

ACKNOWLEDGEMENTS

We wish to acknowledge the helpful assistance afforded our effort by all the people associated with the linac activities at Brookhaven National Laboratory, Los Alamos Scientific Laboratory, Argonne National Laboratory, and the Physical Sciences Laboratory of the University of Wisconsin.

At NAL, the operation of this first section of the linac has been a laboratory goal of high priority and many people have contributed unselfishly of their time and talents. The construction of the linac has been chiefly the responsibility of the engineering members of the NAL Linac Section. The responsibility for mechanical systems has been as follows: M. L. Palmer, drift tubes; J. E. O'Meara,
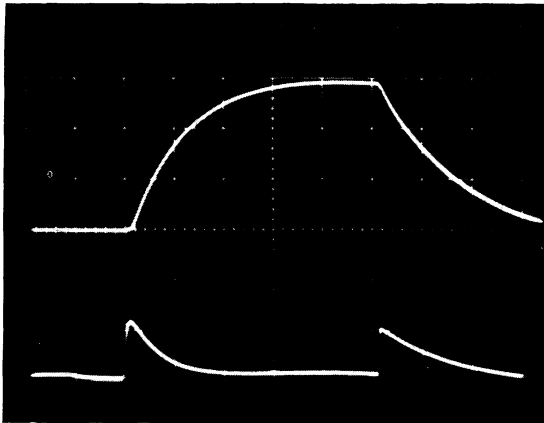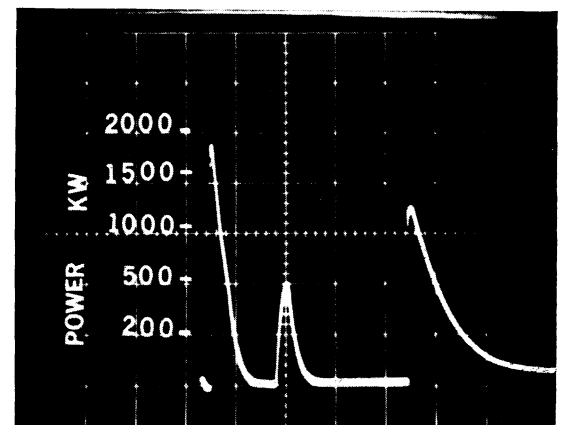
(a) Cavity field buildup and P.A. reverse power with amplitude servo loop open.
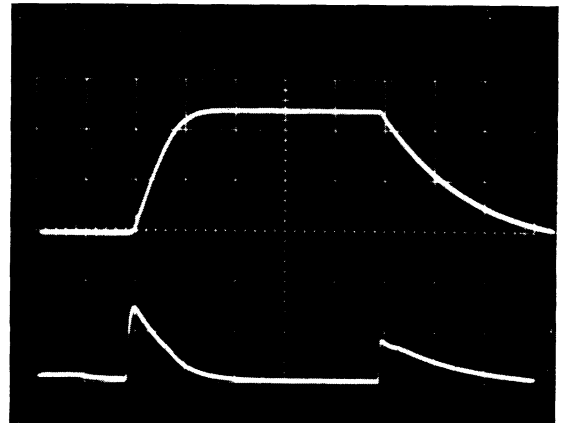
(b) Same as (a) with amplitude servo loop closed.
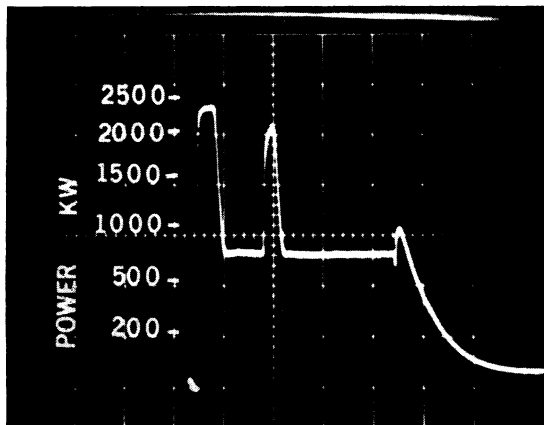
(c) P.A. forward power as seen by calibrated directional coupler with 150 mA at 10.4 MeV.

(d) P.A. reverse power at same conditions as (c).

FIG. 21. RF waveforms showing effects of amplitude servo.

accelerating cavities and vacuum systems; G. M. Lee, preaccelerator and beam transport; F. M. Krzich, water systems; J. D. Hogan, alignment. L. J. Sobocki and A. E. Skraboly, design-drafting. Electrical-engineering responsibilities have been as follows: R. A. Winje and J. S. Bobbitt, rf systems; R. P. Featherstone, electronic systems; E. W. Anderson, computer hardware; N. J. Lau, computer hardware and software; A. R. Donaldson, timing systems; and D. I. Mendenhall, rf equipment. We acknowledge our debt to them and to all the other members of the Linac Section who have worked unstintingly to achieve our common goals. We also are grateful to individuals in other sections of the laboratory for their support and encouragement in this effort.

REFERENCES

1. National Accelerator Laboratory Design Report, July 1968.
2. Staff, AGS Conversion Division, Brookhaven Accelerator Department, 'Alternating-Gradient Synchrotron Conversion Program', BNL 9500 (1965); G. W. Wheeler, 'Progress Report on the AGS Conversion Project', *Proceedings of the Sixth International Conference on High Energy Accelerators 1967, Cambridge, Mass.*, CEAL-2000, p. 414.
3. D. A. Swenson, E. A. Knapp, J. M. Potter and E. J. Schneider, 'Stabilization of the Drift Tube Linac by Operation in the $\pi/2$ Cavity Mode', *Proceedings of the Sixth International Conference on High Energy Accelerators 1967, Cambridge, Mass.*, CEAL-2000, p. 167.
4. J. A. Fasolo, C. D. Curtis and G. M. Lee, 'Duoplasmatron Source Performance at MURA', *Proceedings of 1966 Linear Accelerator Conference, Los Alamos, New Mexico*, LA-3609, p. 371.

5. Th. J. M. Sluyters and V. J. Kovarik, 'Large Brightness Beam Up to 200 mA in a 750 kV High Gradient Preinjector', *Proceedings of the Sixth International Conference on High Energy Accelerators 1967, Cambridge, Mass.*, CEAL-2000, p. 275.

6. G. M. Lee and C. D. Curtis, 'High Gradient Accelerating Column Design and Construction', IEEE Trans. Nucl. Sci., **NS-14,** No. 3, 129 (1967).

7. C. Curtis, E. Gray, P. Livdahl, C. W. Owen, M. Shea, D. Young, 'The Operation of the First Section of the 200 MeV Linear Accelerator for the 200 GeV Synchrotron', *Proceedings of the Seventh International Conference on High Energy Accelerators 1969, Yerevan, U.S.S.R.* (to be published).

8. R Chasman, 'Numerical Calculations of the Effects of Space Charge on Six Dimensional Beam Dynamics in Proton Linear Accelerators', *Proceedings of the 1968 Proton Linear Accelerator Conference*, BNL 50120, p. 372.

9. B. Austin, T. W. Edwards, J. O'Meara, M. L. Palmer, D. A. Swenson, and D. E. Young, 'The Design of Proton Linear Accelerators for Energies Up to 200 MeV', MURA 713 (1965) (unpublished).

10. J. O'Meara and M. Palmer, 'Mechanical Design Features of the NAL 200 MeV Linac Injector', *Proceedings of the 1968 Proton Linear Accelerator Conference,* BNL 50120, p. 30.

11. C. W. Owen, C. A. Radmer and D. E. Young, 'RF Perturbation Measurements in Long Linac Cavities', *Proceedings of the 1966 Linear Accelerator Conference, Los Alamos, New Mexico*, LA 3609, pp. 140–145.

12. Developed and built by Continental Electronics Manufacturing Company of Dallas, Texas.

13. Xerox Data Systems Sigma II.

14. C. S. Taylor, D. J. Warner, F. Block and P. Tetu, 'Progress Report on the CERN-PS Linac'. *Proceedings of the 1966 Linear Accelerator Conference, Los Alamos, New Mexico*, LA 3609, pp. 48–59.

15. D. A. Swenson and J. E. Stovall, 'PARMILA', LASL Report No. MP-3-90 (1969) (Unpublished).